Microbial-mediated bastnaesite dissolution as a viable source of clay-adsorbed rare earth elements in the regolith-hosted deposits

Yilin He[a,b,d], Lingya Ma[a,c,*], Xurui Li[a], Xun Liu[a,b], Xiaoliang Liang[a,b], Jianxi Zhu[a,b], Hongping He[a,b]

[a] State Key Laboratory of Deep Earth Processes and Resources/Guangdong Provincial Key Laboratory of Mineral Physics and Materials, Guangzhou Institute of Geochemistry, Chinese Academy of Sciences, Guangzhou 510640, PR China

[b] University of Chinese Academy of Sciences, Beijing 100049, PR China

[c] State Key Laboratory of Critical Earth Material Cycling and Mineral Deposits, School of Earth Sciences and Engineering, Nanjing University, Nanjing, Jiangsu 210023, PR China

[d] GFZ Helmholtz Research Center for Geosciences, Potsdam 14473, Germany

*Corresponding author. Email address: lingya.ma@nju.edu.cn (Lingya Ma).

Abstract

Understanding the weathering processes of minerals containing rare earth elements (REE) is crucial for unraveling the genesis of regolith-hosted REE deposits. However, the weathering mechanisms of bastnaesite, a primary REE carrier in parent rocks, remain uncertain. Discrepancies between field observations and thermodynamic calculations regarding its weatherability during mineral-groundwater interactions have raised questions about the factors controlling the natural weathering of bastnaesite. Here, we propose that microbial activities significantly contribute to the dissolution of bastnaesite. To test this hypothesis, we conducted bio-weathering experiments using natural bastnaesite and a wild strain, *Bacillus thuringiensis* (Bt) isolated from regolith-hosted REE deposits. The results indicate that, consistent with thermodynamic predictions, bastnaesite exhibited resistance to dissolution under simulated groundwater pH conditions (~6). However, the presence of Bt significantly enhanced bastnaesite dissolution. Bt exuded various types of organic acids, acidifying the solution during bio-weathering. Comparative biotic and abiotic experiments demonstrated that Bt could induce bastnaesite dissolution through acidolysis and ligand complexation. These effects were further strengthened by direct cell attachment to the mineral surfaces. Existing field studies suggest the rapid dissolution of bastnaesite during the very early rock weathering period, adding uncertainty about the contribution of bastnaesite to the enrichment of clay-adsorbed REE. Our results indicate that the dissolution of bastnaesite is largely pH-dependent, with bio-dissolution rates (R_{Ce} = 10^{-13}–10^{-12} mol·m^{-2}·s^{-1}) close to or slightly lower than the lab-determined dissolution rates of feldspars and micas at weakly acidic to neutral pH levels. Since the weathering of these aluminosilicate minerals provides the dominant source of clay minerals, we infer that some

REE released from bastnaesite can be retained by clay minerals in the weathering profile. These findings may provide new insights into the natural weathering of bastnaesite and advance our understanding of the REE biogeochemical cycling during the formation of regolith-hosted REE deposits.

***Keywords*:** bastnaesite, bio-weathering, *Bacillus thuringiensis*, REE mobilization, regolith-hosted REE deposits

1. Introduction

Rare earth elements (REE) include the 15 lanthanides, as well as Y and Sc. REE fluorcarbonates, one of the largest groups of REE minerals, ubiquitously occur in various types of REE deposits (Migdisov et al., 2016), including carbonatite-related (Guo and Liu, 2019), breccia-hosted (Williams-Jones et al., 2000), and regolith-hosted REE deposits (Li et al., 2022a; Sanematsu et al., 2013; Yang et al., 2023). Bastnaesite [$REE(CO_3)F$], as the dominant member of REE fluorcarbonates, is among the most economically important REE resources. This has sparked considerable interest in the physicochemical conditions controlling their formation (Shivaramaiah et al., 2016; Williams-Jones and Wood, 1992). However, the supergene alteration of these minerals remains poorly understood, even though they are closely linked to the development of critical and strategic regolith-hosted REE resources (Li et al., 2022a; Sanematsu et al., 2013; Shi et al., 2024), which contribute more than 15% of the worldwide REE supply (Li et al., 2020).

The mobilization of REE primarily from the accessory REE phases in parent rocks, followed by their downward transport during meteoric water leaching, and subsequent sorption mainly by clay minerals result in gradual REE enrichment in the weathering profiles and the formation of regolith-hosted REE deposits (Borst et al., 2020; Li et al., 2019a; Shi et al., 2024). This transformation enables easier REE recovery using dilute electrolyte solutions (*e.g.*, ammonium sulfate solutions) without mineral processing, thereby greatly reducing extraction costs and leading to higher economic benefits (Sanematsu and Watanabe, 2016). Consequently, understanding the dissolution of REE carrier minerals is essential for revealing the mineral source of clay-adsorbed REE and comprehensively modeling the development of economic regolith-hosted REE deposits.

Current knowledge about the stability of many REE-bearing minerals in supergene weathering environments is largely derived from field investigations combined with empirical conjecture (Li et al., 2022a; Sanematsu et al., 2013; Sanematsu and Watanabe, 2016). For example, REE fluorcarbonate minerals are generally inferred to be easily dissolved during the early period of weathering, as they are found in the parent rock but are rarely observed in the semi-weathered zone (Huang et al., 2021b; Sanematsu et al., 2013). The typically weakly acidic weathering profiles of the regolith-hosted deposits formed by subtropical weathering as well as the susceptibility of carbonate to acid dissolution (Borst et al., 2020; Li et al., 2022a; Morse and Arvidson, 2002), also provide plausible justification for this speculation. However, thermodynamic calculations regarding fluorcarbonate stability in regolith-hosted REE deposits yield conflicting results that fluorcarbonate minerals, such as bastnaesite, are predicted to be resistant to dissolution in acidic environments (pH = 5.4−6) (Li et al., 2022a). This contradiction prompts the question of what are the factors responsible for the dissolution of bastnaesite in the weathering profile.

The above-mentioned thermodynamic calculation, only considered dissolution reactions in inorganic systems (Li et al., 2022a), overlooking the potential effects of microbial activities in the profile (Li et al., 2022b), which have been acknowledged as significant driving factors for mineral weathering (Dong et al., 2022; Wild et al., 2022). Unfortunately, the bio-weathering of REE fluorcarbonate minerals has rarely been determined, possibly due to their occurrence as accessory minerals in trace amounts, making them difficult to be separated from the bulk rock for dissolution experiments (He et al., 2023; Sanematsu et al., 2013; Shi et al., 2024). To date, only Zhang et al. (2018),

aiming to establish a cost-effective green technology for recovering REE from low-grade ores, investigated REE bioleaching from bastnaesite-bearing rocks by actinobacteria from a carbonatite-related REE deposit. The inherent challenge in elucidating the behavior of REE released from different phases within a complex network of interactions among different minerals or elements in the rocks warrants attention (Kelly et al., 2016). These interactions may affect REE behavior during mineral dissolution, as well as the interpretation of bio-weathering mechanisms, which may vary in specificity and efficacy towards different geological substrates (Samuels et al., 2020). Therefore, the dissolution of REE fluorcarbonate minerals in the presence of microbes and the underlying mechanisms still need further study.

In this context, we propose that microbial activities may drive the natural dissolution of REE fluorcarbonates, making them viable sources of clay-adsorbed REE in the regolith-hosted REE deposits. Given that the living environment may mold the metabolic activities and functions of microbes, a native strain from a regolith-hosted REE deposit was used in the bio-weathering experiments. To reduce the geological complexity and explore bio-weathering mechanisms in more detail (Kelly et al., 2016), high-purity bastnaesite was employed in our experiments to examine mineral dissolution and the associated mechanisms. This also enables us to quantify the dissolution rates of bastnaesite under simulated weathering conditions representative of regolith-hosted REE deposits. By comparing these dissolution rates to those of feldspars (plagioclase and K-feldspars) and micas (biotite and muscovite), we further revealed the effective contribution of bastnaesite to clay-adsorbed REE. Our findings provide plausible explanations for the discrepancies between field observation and theoretical simulation of bastnaesite weathering and help

112 improve the understanding of REE biogeochemistry during the formation of regolith-
113 hosted REE deposits.
114

115 **2. Materials and methods**

116 **2.1 Mineral sample preparation and characterization**

117 The bastnaesite mineral sample used in this study was selected from bastnaesite-
118 bearing rock collected from the Maoniuping giant REE deposit, in western Sichuan
119 Province, China (Weng et al., 2022). The selected bastnaesite mineral grains were crushed
120 in an agate mortar and sieved to obtain the 48−74 μm fractions. After that, the mineral
121 powders were washed more than 10 times to remove fine particles adhering to mineral
122 surfaces and then freeze-dried. Semiquantitative X-ray powder diffraction analysis (XRD),
123 performed using a Rigaku MiniFlex-600 X-ray diffractometer equipped with Ni-filtered
124 CuKa radiation, verified that the bulk sample is composed of ~97 wt% bastnaesite and ~3
125 wt% quartz (Fig. 1). The chemical compositions of the prepared mineral samples were
126 determined by X-ray fluorescence spectrometry (XRF; Axios Adv PW4400, PANalytical,
127 Netherlands) and inductively coupled plasma mass spectrometry (ICP-MS; Agilent 7900,
128 Agilent, USA). The total amount of LREE (from La to Nd) oxides is ~76% with La and Ce
129 being the dominant REE components (Table 1). The average specific surface area of the
130 prepared mineral sample was determined by Brunauer, Emmett, and Teller (BET) analysis
131 (ASAP2020, Micromeritics, USA).
132

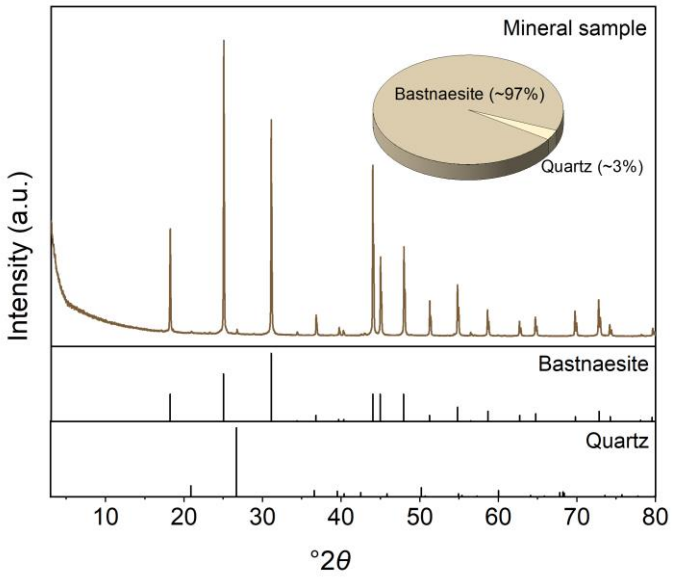

Fig. 1. XRD pattern of the bastnaesite sample and the calculated mineral compositions following the methods shown in Supplementary Text S2.

2.2 Microbial inoculum preparation

Bacillus thuringiensis (Bt) was isolated from the Renju regolith-hosted REE deposits in Guangdong Province, South China. The microbial isolation and identification procedures were elaborated in our previous work (He et al., 2024). Bt is widely distributed in natural environments and can be easily laboratory pure-cultured. It also exhibits great performance in the bio-weathering of REE minerals (He et al., 2024) and can survive in oligotrophic laboratory media containing bastnaesite. These are prerequisites for our experiment. Before experiments, Bt was pre-cultivated on Luria-Bertani (tryptone 10 $g \cdot L^{-1}$, yeast extract 5 $g \cdot L^{-1}$, NaCl 10 $g \cdot L^{-1}$, and agar 15 $g \cdot L^{-1}$) medium plates, harvested at their exponential phase, washed with sterile ultrapure water, and then resuspended in fresh experimental media.

2.3 Mineral dissolution experiments

2.3.1 Biotic dissolution experiments

To ascertain whether the microbial strain can cause pH change (Liermann et al., 2000) and more closely simulate natural conditions (Goyne et al., 2010), modified unbuffered media (1.0 $g \cdot L^{-1}$ $MgSO_4 \cdot 7H_2O$, 0.2 $g \cdot L^{-1}$ KCl, 1.0 $g \cdot L^{-1}$ NH_4Cl, 10 $g \cdot L^{-1}$ glucose, pH = 6) was used (Brisson et al., 2020; He et al., 2024). For comparison, media buffered by 20 $mmol \cdot L^{-1}$ 2- [N-morpholino] ethane sulfonic acid (MES) were used to examine mineral dissolution at constant pH = 6 (Kalinowski et al., 2000). Due to the high affinity between REE and P, the addition of P-containing reagents in the media was avoided to reduce their effects on REE behavior during mineral dissolution (Feng et al., 2011; Goyne et al., 2010). Bacteria were expected to obtain trace P from minerals or use the products of cell metabolism and dead cell lysis (Laměrand et al., 2020). All utensils and solutions were sterilized in advance by autoclaving at 121°C for 30 min or filtrating with 0.22-μm filters. In biotic dissolution experiments using unbuffered (Exp-Biow) and buffered (Buffered-Biow) media, 250 mL flasks containing 100 mL of liquid media and 0.5 g of mineral powders were inoculated with 100 μL of Bt cell suspensions. The final cell concentrations were ~10^6 $CFU \cdot mL^{-1}$. Dissolution experiments without Bt (Exp-Sterile and Buffered-Sterile) and pure culture of Bt without minerals (Exp-Bt and Buffered-Bt) were performed as controls in both unbuffered and buffered media. Additionally, to examine the potential impact of cell attachment on bastnaesite dissolution, dialysis bags (10 K MWCO, 35 mm, Thermo Fisher Scientific, USA) were used to inhibit direct contact between microbial cells and the mineral sample (Fathollahzadeh et al., 2018; Sheng et al., 2023). The mineral samples were enclosed in dialysis bags (Exp-bags) and other experimental set-ups were the

same as those in the unbuffered bio-weathering experiment (Exp-Biow). All operations were carried out in an aseptic workbench. All flasks were incubated on an orbital shaker at 180 rpm, room temperature for 30 days.

At different time intervals, 1.5 mL of suspensions were sampled from triplicate reactors for solution pH, aqueous elemental concentrations, and cell density analyses. To better reduce artificial interference, suspensions sampled from the unbuffered media on days 4, 8, and 15 were used for metabolomic analysis (Brisson et al., 2020). Additional replicates of the Exp-Biow and Exp-Bt groups were performed for metabolomic analysis, respectively. Briefly, 1 mL of cell culture was collected, centrifuged at 4°C (1000 g, 10 min), and filtered through 0.22-μm syringe filters to remove cells. The filtrates were immediately quenched in liquid nitrogen for 30 s and stored at −80°C.

2.3.2 Abiotic dissolution experiments

Abiotic dissolution experiments were performed to verify the effect of pH and microbial-exuded organic acids. 0.1 g mineral samples and 20 mL HCl or organic acid (1 or 0.02 $mmol \cdot L^{-1}$) solutions were added in sterile 50 mL polypropylene tubes. The organic acids used in this study are summarized in Table S1. The initial solution pH was set at 3, 5, and 6 to mimic the pH range measured in the bio-weathering experiments and the pH range of weathering profiles (Huang et al., 2021a). All solutions were filtered through 0.22-μm filters to exclude microbial contamination. The tubes were shaken horizontally at 180 rpm and room temperature. To better characterize REE release at the initial stage of mineral dissolution, solution pH and dissolved elemental concentrations were analyzed at the end of 96 h incubation (Zhang et al., 2018).

193 ***2.3.3 Analyses***

194 The solution pH was measured with a pH meter (FiveEasy Plus™, Mettler-Toledo,
195 USA) equipped with a micro pH electrode (LE438, Mettler-Toledo, USA). Conventional
196 ager plate counting was performed to evaluate the living cell densities (Sarrah and You,
197 2019). The quantified cell density only refers to planktonic cells and the cells attaching to
198 mineral surfaces are not included. Aqueous elemental concentrations were analyzed using
199 an inductively coupled plasma mass spectrometer (ICP-MS; iCAP Qc, ThermoFisher
200 Scientific, USA). Briefly, all solutions are filtered through 0.22 μm membranes and then
201 diluted in 2% HNO_3. All certified reference materials were purchased from AccuStandard,
202 USA. Standard materials, including MISA-01–1, ICP-MS-CAL2-1, and ICP-MS-CAL4-1
203 were used to establish calibration lines. The internal standard was 20 $\mu g \cdot L^{-1}$ Rh solution
204 (ICP-MS-IS-RH-1). According to established protocols (He et al., 2024), metabolomic
205 analysis was performed on an ultra-performance liquid chromatograph system (UHPLC;
206 Vanquish, Thermo Fisher Scientific) coupled with an Orbitrap Exploris 120 mass
207 spectrometer (Orbitrap MS, Therm) at Guangdong Magigene Biotechnology Co., Ltd.,
208 China. Details of metabolite extraction, analyses, and data processing are shown in
209 Supplementary Text S1. As for the resulting solids, XRD analysis was conducted to verify
210 any mineralogical change. Morphological and compositional analyses were performed on
211 a TESCAN MIRA3 field-emission SEM equipped with EDS at 20 kV, after Au or C coating.
212 To preserve the textural relationship between microbes and minerals, the solid samples
213 were fixed in 2% paraformaldehyde and 2.5% glutaraldehyde solutions and ethanol
214 gradient dehydration. In addition, to avoid interference during sample preparation, portions
215 of the collected suspensions without pre-treatment were directly dropped onto conductive

tapes and air-dried for SEM analyses at 3 kV.

3. Results

3.1. Cell density, pH variation, and organic acid metabolism

The variation of cell densities was roughly similar across different treatments (Fig. 2A), with an initial increase followed by either a decrease or plateau. Specifically, in unbuffered media (Exp-Biow & Exp-Bt), cell densities increased rapidly within the first day followed by a sharp decrease and then maintained at around 5 and 3 ($\times 10^6$ CFU·mL^{-1}), respectively in cultures with and without bastnaesite. In buffered media (Buffered-Biow), Bt experienced exponential growth during the first 6 days followed by a stationary phase with cell densities in the range of 7−8 ($\times 10^6$ CFU·mL^{-1}). In dissolution experiments using dialysis bags (Exp-bags), cell densities were slightly lower than those in the Exp-Biow group without dialysis bags, slightly decreasing to ~3 ($\times 10^6$ CFU·mL^{-1}) between days 1 to 30.

The proliferation and metabolism of Bt resulted in significant acidification of the unbuffered media (Fig. 2B). The solution pH in Exp-Biow and Exp-Bt groups decreased by more than 1 unit within the first day. Subsequently, the pH of the Exp-Biow group decreased at a faster rate, reaching the lowest level by day 10, and maintaining at ~3.5 for the remainder of the experiment. The pH of the Exp-Bt group steadily decreased between days 1 to 30, and the lowest pH was ~3.7. In dissolution experiments using dialysis bags (Exp-bags), the solution pH underwent a sharp decrease within the first day, then slowly dropped to the minimum of ~4.3 on day 4. Thereafter, the solution pH maintained around this level with a slight upward trend, in line with the observed variation in cell densities

(Fig. 2A). The pH value of Exp-Control and Buffered-Biow groups remained at around 6 throughout the experiments.

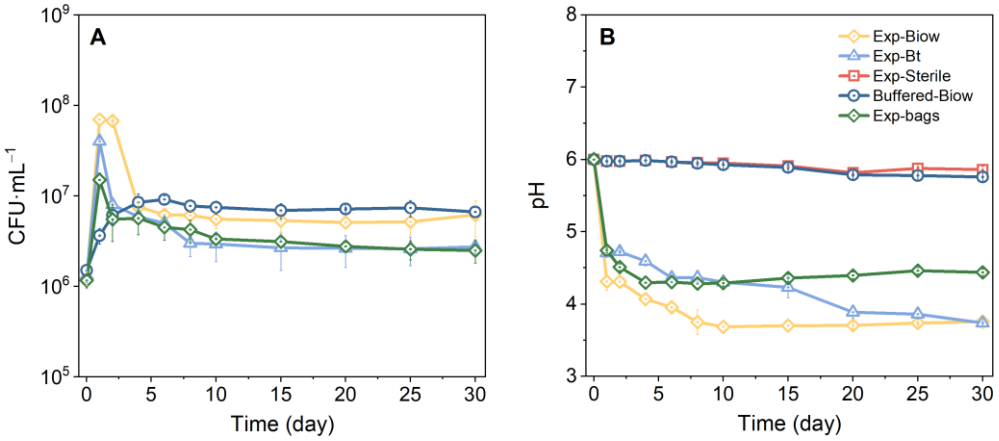

Fig. 2. Variation of cell densities (A) and solution pH (B). Error bars indicate the standard deviation of triplicates.

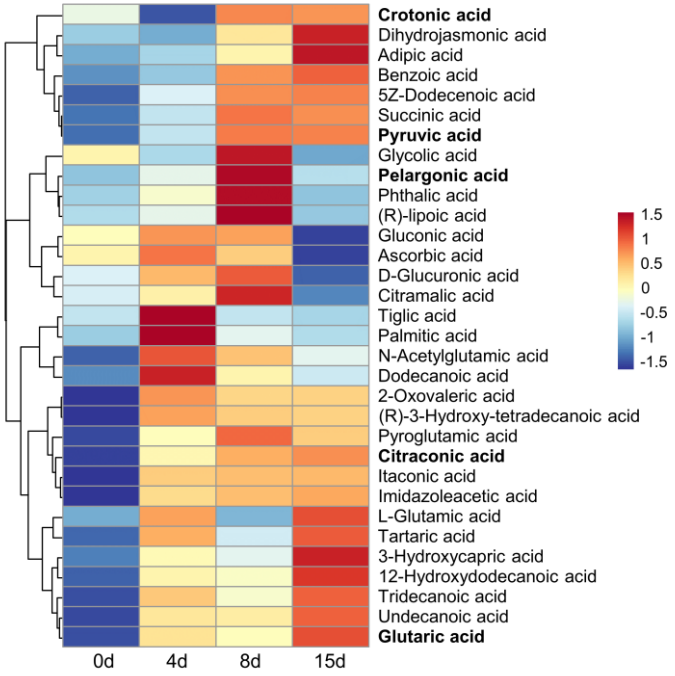

Fig. 3. Concentration profiles of 32 organic acids of interest. The concentrations were normalized using internal standards. The heatmap shows average levels of identified metabolites detected during experiments for each time point. The scale bar represents the log2-transformed and z-score-normalized ratios. The names of organic acids in higher concentrations (average normalized concentration > 2 at each time point) are given in bold.

Metabolomic data show that Bt produced more than 5000 metabolites but only 111 of them can be identified with chemical names (shown in Research Data). Particular attention is given to organic acids due to their widespread occurrence and essential roles in bio-weathering (Dong et al., 2022; Li et al., 2021) and REE bioleaching (Zhang et al., 2018; Brisson et al., 2020). Identifying these metabolites as known compounds is a prerequisite for further laboratory examination of their leaching abilities. Therefore, we focused only on the identifiable organic acids. The concentration profiles of 32 organic acids of interest are summarized in Fig. 3. The majority of these organic acids are commonly produced during microbial metabolism and detected in soils (Li et al., 2021; He et al., 2024). The concentrations of these organic acids on days 4, 8, and 15 were higher than those in the media control (t = 0 d). Organic acids of potential bio-weathering importance were identified through the approaches proposed by Brisson et al. (2020). Firstly, organic acids with higher abundance were selected. Here, an average internal standard normalized concentration > 2 at each time point (days 4, 8, and 15) was used as a screening criterion. Consequently, crotonic, pyruvic, pelargonic, citraconic, and glutaric acids were screened out (Fig. 3). Secondly, driven by nutritional needs, microbes might activate the metabolism of efficient weathering agents to extract elements from minerals (Brisson et al., 2020; Schmalenberger et al., 2015). There is no significant difference in the overall metabonomics of Bt in the presence or absence of bastnaesite. Despite no compound being unique to the Bt co-culture with bastnaesite, up-regulation of some metabolites was detected in the culture with bastnaesite in comparison to the pure culture, including organic acids, which was also in line with the accelerated solution acidification (Fig. 2B). Therefore, we focused on organic acids with significantly higher concentrations in the co-culture of

Bt and bastnaesite (Exp-Biow) compared to the pure culture of Bt (Exp-Bt). The screening criteria were P-value < 0.05, VIP > 1, and Fold change ≥ 2. As a result, 4 organic acids were identified, including itaconic, benzoic, succinic, and pyruvic acids (Fig. 4). The 8 identified organic acids of potential bio-weathering importance are summarized in Table S1. Only 7 of them were used for further abiotic leaching experiments because pelargonic acid is insoluble in water under experimental conditions.

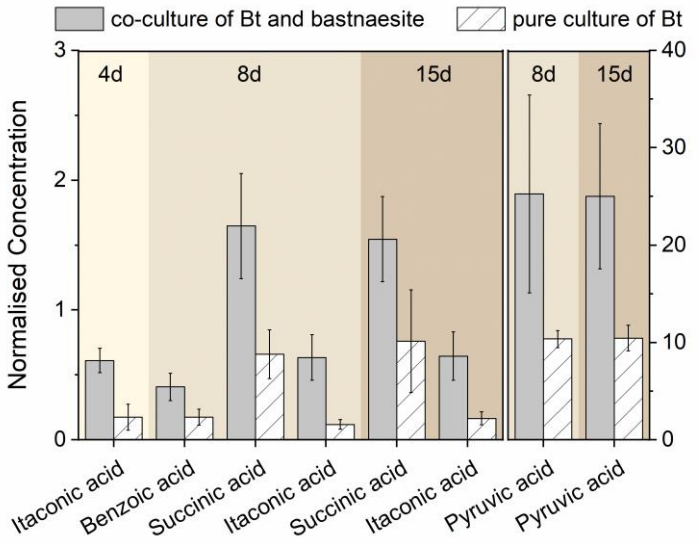

Fig. 4. Organic acids of potential bio-weathering importance identified by their occurrence at higher concentrations in the co-culture of Bt and bastnaesite compared to the pure culture of Bt at certain time points. Screening criteria: P-value < 0.05, VIP > 1, Fold change ≥ 2. Error bars indicate the standard deviation of sextuplicate (co-culture of Bt and bastnaesite) or quintuplicate (pure culture of Bt).

3.2. Bastnaesite dissolution and REE mobilization

Solution chemistry data support the dissolution of bastnaesite enhanced by Bt (Fig. 5). The concentrations of aqueous REE measured in control groups (Exp-Control, Buffered-Control, Exp-Bt, and Buffered-Bt) were close to the detection limits of ICP-MS. In the presence of Bt, the concentrations of dissolved REE continuously increased during the 30-

294 day experiments (Fig. 5). In unbuffered media, the highest amounts of aqueous REE were
295 ~1698 μg·L^{-1} (Fig. 5A). Consistent with the chemical compositions of initial bastnaesite
296 sample (Table 1), more than 98% of the dissolved REE were composed of La (~643 μg·L^{-1}),
297 Ce (~805 μg·L^{-1}), Pr (~60 μg·L^{-1}), and Nd (~165 μg·L^{-1}). When buffering the medium pH
298 at 6, the concentrations of aqueous REE decreased and the highest concentration of total
299 REE was ~84 μg·L^{-1} (Fig. 5B). In dialysis bag experiments, Bt was still able to mobilize
300 REE from bastnaesite without direct cell-mineral contact (Fig. 5C), with the highest
301 concentration of total REE being ~490 μg·L^{-1}. The ratio of LREE relative to the total REE
302 (LREE/REE) is used to better characterize the potential incoherent release of different
303 groups of REE, due to the extremely high concentrations of LREE in bastnaesite. In
304 comparison, the ratios of dissolved LREE/REE in different treatments were slightly lower
305 than the LREE/REE ratio of the initial bastnaesite sample (~1.00) (Fig. S1). The slightly
306 higher mobility of HREE relative to LREE during the early stage of bastnaesite dissolution
307 simulated in our experiments may be related to the lower compatibility of HREE with the
308 crystal structure of bastnaesite (Shibata et al., 2006) or the preferential mobilization of
309 HREE relative to LREE through bacterial weathering (He et al., 2023). Here, we did not
310 further explore the factors controlling the incoherent mobilization of LREE and HREE
311 under different treatments because such a slight preferential release of HREE holds limited
312 practical significance. The compositions of released REE are substantially inherited from
313 the original bastnaesite, so the input of dissolved LREE into the environment is far higher
314 than that of HREE during bastnaesite dissolution.

315 The concentrations of REE leached from bastnaesite by HCl and organic acids
316 selected in Section 3.1 were illustrated in Fig. 6A. At pH = 3, the REE concentrations

leached by organic acids (~1915−2180 μg·L^{-1}) were close to that leached by HCl solutions (~1993 μg·L^{-1}). At pH = 5, the tested organic acids (~343−579 μg·L^{-1}) showed higher REE leaching efficiency than the HCl solution (~328 μg·L^{-1}). When the initial pH was increased to 6, neither the selected organic acids nor HCl solution successfully mobilized REE.

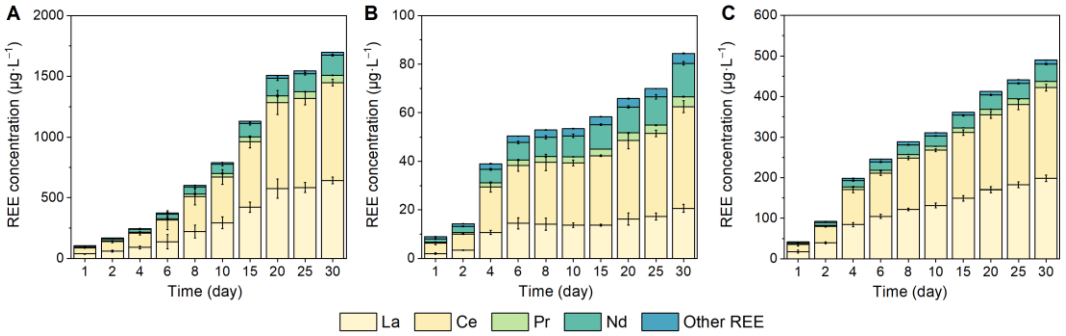

Fig. 5. The aqueous REE concentrations throughout the 30-day unbuffered (A), buffered (B), and dialysis bag (C) experiments. Error bars indicate the standard deviation of triplicates.

4. Discussion

4.1. Mechanisms of microbial-enhanced REE mobilization from bastnaesite

The microbial strain survived in the experimental media throughout the 30-day experiments (Fig. 2A), possibly using the products of living cell metabolism, dead cell lysis, or bastnaesite dissolution as sources of nutrients (Lamérand et al., 2020). The cell densities increased to different extents compared to the initial values but the increments were less than one order of magnitude, suggesting that the available nutrients were sufficient to maintain the viability of bacteria but not to stimulate significant proliferation (Lamérand et al., 2020). In bio-weathering systems, living cell metabolic activities are the primary drivers of pH decrease (Ahmed and Holmström, 2015; Li et al., 2019b). The continuous

pH decrease in the Exp-Biow group indicates that living cell metabolism is the dominant control of solution pH. Therefore, although thriving cell growth was not observed (Fig. 2A), our experimental systems still can reflect the interactions between living bacteria and bastnaesite.

4.1.1 Acidolysis and ligand complexation

Acidolysis and ligand complexation have been recognized as the primary mechanisms employed by heterotrophic microbes to induce mineral dissolution during bio-weathering (Wild et al., 2022). In our bio-weathering experiments, Bt exuded various kinds of organic acids and significantly acidified the solution (Figs. 2B & 3). Organic acids play a central role, supplying both protons and ligands. Ligand-induced complexation can increase the concentration of dissolved REE primarily through forming surface complexes to detach structural REE from the mineral surface and complexing aqueous REE to disrupt equilibria at the mineral-solution interface and enhance mineral dissolution to restore equilibrium (Samuels et al., 2020). In this study, the dissolved REE concentrations generally increased as a function of decreasing pH in both biotic (Figs. 2B & 5) or abiotic systems (Fig. 6A). At pH = 5, the higher REE leaching efficiencies of organic acids compared to the HCl solution indicating the involvement of ligand-promoted dissolution (Fig. 6A). When the initial pH was increased to 6, neither the selected organic acids nor HCl solutions successfully mobilized REE (Fig. 6A), however, Bt was still capable of inducing bastnaesite dissolution (Fig. 5B). This suggests that the stronger organic acid ligands exuded by Bt may be responsible for the REE release at pH = 6. To further investigate this possibility, we additionally examined the bio-weathering potential of tartaric and gluconic acids produced by Bt (Figs. 3 & 7B). REE release efficiencies by different organic acids

are primarily determined by their complexing stability with REE (He et al., 2023; Goyne et al., 2010). These two organic acids, which contain multiple -COOH and -OH groups can form more stable chelates with metals (Konhauser, 2007). The results confirm that tartaric and gluconic acids could liberate REE from bastnaesite even at pH = 6 and a low concentration (20 μM) (Fig. 6B). Overall, bastnaesite dissolution is largely pH-dependent, but ligand-promoted complexation plays an important role at pH ≥ 5. This pH range corresponds to conditions typically found in the weakly-weathered zone, where REE fluorcarbonates are dissolved in large quantities (Huang et al., 2021a, b).

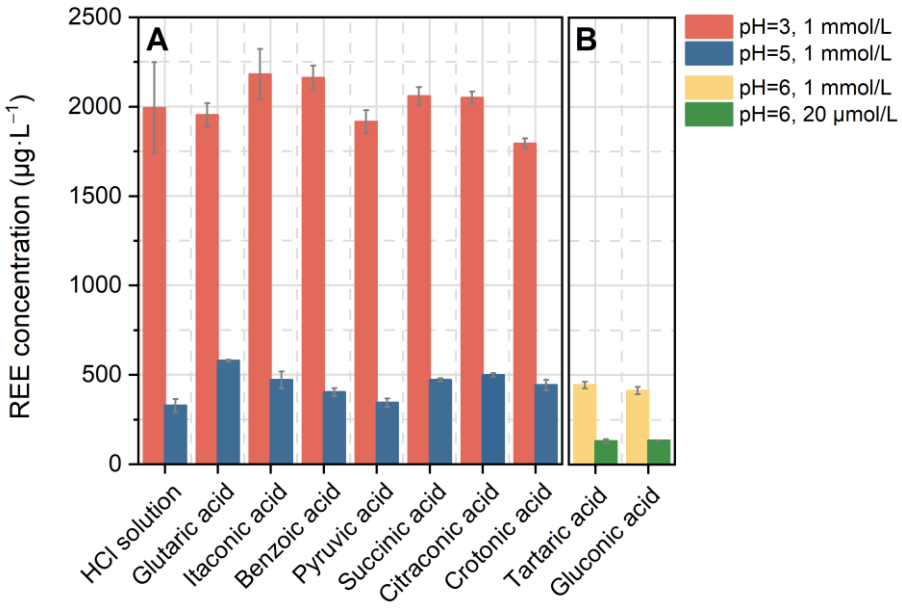

Fig. 6. Concentrations of REE leached from bastnaesite by HCl and selected organic acid solutions. Error bars indicate the standard deviation of triplicates.

4.1.2 Potential positive effects of cell attachment on mineral surfaces

Microbial colonization occurred on the bastnaesite particle surfaces during incubation, leading to the formation of erosion features and secondary precipitates formed in the vicinity of cells (Fig. 7). These alteration features were absent in the original mineral grains

with clean and smooth surfaces, as well as the mineral samples in the abiotic dissolution experiments. Consequently, these features were interpreted as the result of microbe-enhanced mineral dissolution (Lamérand et al., 2020). The newly formed precipitates exhibited a loose and fine morphology, but their chemical compositions closely resembled those of initial bastnaesite (Fig. 7E & F). The XRD results also verified that there was no obvious mineralogical phase change after the 30-day incubation (Fig. S2). One possible explanation is that microbial colonization could promote the detachment of REE while reducing the local water/solid ratio, thereby inducing the localized reprecipitation of the released elements (Benzerara et al., 2005). Similar secondary REE fluorcarbonates have also been found in natural deposits as intermediate products. As weathering progresses, these secondary phases can be eventually dissolved (Yang et al., 2023).

When direct microbial colonization on mineral surfaces was inhibited by dialysis bags, the concentrations of released rare earth elements (REE) decreased (Fig. 5), even at similar cell density levels (Fig. 2A), indicating that cell attachment favored mineral dissolution. Bacterial colonization on mineral surfaces may occur either by chance or as a deliberate strategy to exploit this specific niche (Dong et al., 2022) to cope with environmental stress (Rather et al., 2021) or acquire inorganic nutrients (Uroz et al., 2011). Previous studies have reported a strong correlation between microbial colonization and dissolution rate (Bennett et al., 1996; Davis et al., 2007). Particle-attached bacteria tend to have a higher proportion of cells with higher metabolic activity than suspending free-living bacteria (Flemming and Wuertz, 2019). Additionally, higher local concentrations of protons and ligands within the micro-scale environment formed between cell and mineral surfaces could also further enhance bastnaesite dissolution (Ahmed and Holmström, 2015; Li et al.,

2016; Wild et al., 2022). In our experiments, the enhanced metabolic activity of Bt induced by bastnaesite was reflected by the time course change of cell density and solution pH in cultures with or without cell-mineral contact (Fig. 2). In bio-weathering experiments using dialysis bags, corresponding to the lower and decaying cell density, the solution pH level was about 1 unit higher than that observed in the unbuffered bio-weathering experiments without dialysis bags. Therefore, we infer that direct cell attachment on mineral surfaces is an effective approach for microbes to enhance bastnaesite dissolution.

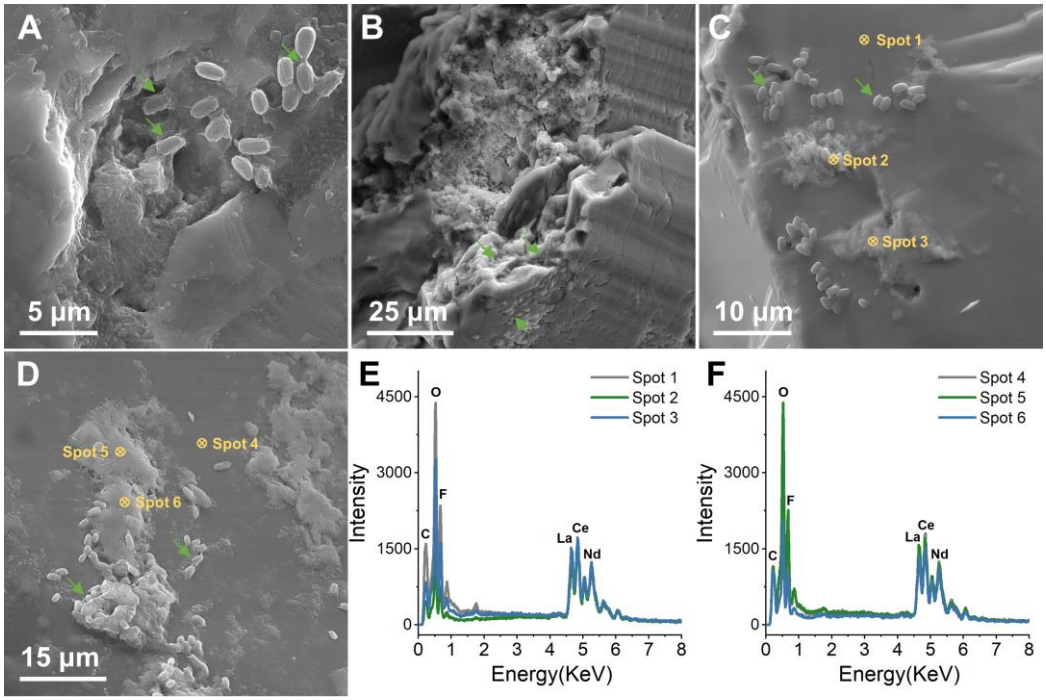

Fig. 7. SEM analyses of bastnaesite mineral surfaces at the end of experiments. SEM-Secondary Electron images showing (A & B) etch pits and (B & D) secondary precipitates in the vicinity of cells. The green arrows point to the bacterial cells. (E & F) The corresponding SEM-Energy dispersive spectroscopy patterns of the points labeled by yellow circles.

4.2. Implications for the contribution of bastnaesite weathering to clay-adsorbed REE

4.2.1 Natural weathering of bastnaesite triggered by microbial activities

The dissolution of bastnaesite and REE liberation from the mineral structure are the prerequisites for bastnaesite to act as a viable source of clay-adsorbed REE. Regarding the discrepancy between natural phenomena and theoretical simulation of bastnaesite dissolution, Li et al. (2022) proposed that the incorporation of radioactive Th and U in natural REE fluorcarbonates may lead to metamictization and reduced mineral stability (Pan and Fleet, 2002). However, our findings suggest that the natural complete weathering of bastnaesite cannot be solely attributed to the distinct chemical compositions of natural versus ideal minerals. Our results show that the natural bastnaesite sample remained resistant to inorganic acid dissolution at a comparable pH level found in regolith-hosted REE deposits (Huang et al., 2021a; Li et al., 2019a), despite its high concentration of Th (Table 1). Surprisingly, REE mobilization from bastnaesite was significantly enhanced in the presence of Bt within the same pH range (Figs. 6 & 7). Therefore, we reasonably highlight the potential role of microbes in accelerating the natural weathering of bastnaesite.

The experimental results indicate that bastnaesite dissolution is largely pH-dependent and also could be enhanced by organic ligand-induced complexation. Microbial activity is one of the main sources of soil acidity and organic ligands. Field observations suggest that the dissolution of bastnasite and other fluorcarbonates begins at the early stage of weathering (*i.e.*, in the lower weathering profile) (Huang et al., 2021b; Sanematsu et al., 2013). Indeed, actively metabolizing microbial populations, including *Bacillus spp.*, have been detected in the nutrient-limited deeper regolith horizons, even at the weathering front, contributing to oxidative rock weathering (Li et al., 2022b; Minyard et al., 2012;

438 Napieralski et al., 2019). Additionally, some organic matter, particularly soluble organic
439 acids, generated by dynamic biological processes in the upper profile, can percolate
440 downward, impacting mineral weathering in the lower profile. The biomass levels in our
441 experiments (Fig. 2A) are also comparable to the average bacterial cell densities in natural
442 soils (10^6–10^9 cells·mL^{-1}), deep subsurface environments (e.g., ~10^5 cells·mL^{-1} in a granite
443 bedrock borehole and ~10^5–10^6 cells·mL^{-1} in deep granitic bedrock fracture fluids), and
444 shallow aquifers (~10^6 cells·mL^{-1}) (He et al., 2023; Shirokova et al., 2012; Purkamo et al.,
445 2016). In addition, the concentration of organic acids in soil solutions typically ranges from
446 0 to 50 μM for di/tricarboxylic acids and from 0 to 1 mM for monocarboxylic acids across
447 a broad range of ecosystems (Adeleke et al., 2017; Strobel, 2001). Our results show that
448 low concentrations (20 μM) of some strong organic ligands (e.g., gluconate and tartrate)
449 are capable of accelerating bastnaesite dissolution (Fig. 6B). In natural environments, over
450 99% of the total microbial biomass colonizes on mineral surfaces (Golubev and Pokrovsky,
451 2006). In the weakly-weathered zone, although the bulk soil pH is near-neutral (6-7) and
452 does not favor bastnaesite dissolution, the pH in the vicinity of metabolizing cells can be
453 more than 1 unit lower than the surrounding environmental pH (Bonneville et al., 2011; Li
454 et al., 2016). Therefore, the microbial effects on bastnaesite dissolution are expected to be
455 significant in the microenvironment between cell and mineral interfaces, where
456 concentrated ligands and low pH conditions prevail (Golubev and Pokrovsky, 2006). Given
457 the prevalence and high activity of heterotrophic organic acids-producing microbes like
458 *Bacillus* in the weathering profile of regolith-hosted REE deposits (Li et al.,2022b), the
459 aforementioned bio-weathering processes may partly account for the natural weathering of
460 bastnaesite in the lower profile. We hypothesize continuous, moderate dissolution of

bastnaesite driven by bio-weathering in the deep profile, with microbial impacts becoming more pronounced over long timescales.

4.2.2 Assessment of the preservation of REE released from bastnaesite by clay minerals

Once REE are released, their preservation within the soil profile is also of great importance. The rapid dissolution of bastnaesite during the early stages of weathering raises another question about the contribution of bastnaesite to the regolith-hosted REE deposits. Clay minerals, the predominant REE reservoir in the profile, are primarily formed by the weathering of rock-forming aluminosilicates, including feldspar and mica group minerals (Borst et al., 2020). Field observations show that as the degree of weathering increases, fluorcarbonates disappear in the upper semi-weathered zone, while some feldspars and micas are still observable, indicating that fluorcarbonates are more susceptible to weathering relative to these aluminosilicates. However, such rapid dissolution may not favor the preservation of the released REE, due to the insufficient amount of clay minerals to act as adsorbents during the early weathering period. To assess the possibility, an evaluation of the weatherability of these minerals is required. Here, we calculate the apparent release rates of REE using the equation (1) as follows (Wu et al., 2008; Xia et al., 2020):

$$R = \frac{dC}{dt} * \frac{V_0}{Am} \qquad (1)$$

Where R ($mol \cdot m^{-2} \cdot s^{-1}$) is the linear release rate, dC ($mol \cdot L^{-1}$) is the variation of aqueous concentration of element, dt (s) is the time interval, V_0 (L) is the volume of the initial solution, m (g) is the mass and A (~0.18 $m^2 \cdot g^{-1}$) is the specific surface area of the bastnaesite sample.

Table 2 shows the release rates of REE in the Buffered-Biow group at a constant pH of 6. The apparent release rates of La, Ce, Pr, and Nd were in the range of 10^{-14}–10^{-12} mol·m^{-2}·s^{-1} (Table 2), while the release rates of other REE were extremely low due to their trace amounts in the mineral sample. Fig. 8 plots the release rates of Ce, as a representative of REE, versus pH under different treatments with stable pH conditions. The release rates of REE in bio-weathering systems are lower than those in the organic acids abiotic leaching systems in this study (Fig. 8). This discrepancy may stem from the lower concentrations of strong organic ligands (*e.g.,* tartrate and gluconate) exuded by Bt compared to those used in the abiotic chemical dissolution experiments. By analogy to our previous bio-weathering experiments involving *Bacillus* spp. under similar conditions (He et al., 2023), we inferred that the release of REE might be underestimated due to cellular scavenging through sorption and precipitation at pH 6. The exact sorption efficiency was not reported in the present study, as the complete separation of cells and minerals in the resulting solids at the end of experiments was not achievable. Additionally, the presence of various metabolites in bio-weathering reactors complicates mineral dissolution reactions. Some metabolites may even inhibit mineral dissolution, resulting in lower bio-weathering efficiency (Balland et al., 2010; Pokrovsky et al., 2021 and references therein).

Here, we compare the dissolution rates of bastnaesite (denoted as R_{Ce}) from this study to those of felspars (plagioclase and K-feldspars) and micas (biotite and muscovite) measured in previous laboratory studies (denoted as R_{Si}) (Fig. 8). These data were obtained from inorganic or organic systems with pH, temperature, or organic concentration levels similar to those in our study (Balogh-Brunstad et al., 2008; Blum and Stillings, 1995; Bray et al., 2015; Gudbrandsson et al., 2014; Heřmanská et al., 2022; Kalinowski and Schweda,

1996; Lammers et al., 2017; Stillings et al., 1996; Voinot et al., 2013; Welch et al., 1999; Wolff-Boenisch et al., 2006 and references therein). The dissolution of both aluminosilicates and bastnaesite is pH-dependent so the dissolution rates are plotted against pH (Fig. 8). The considerable scatter in the dissolution rates of the aluminosilicates may stem from the differences in experimental set-ups (*e.g.*, solid/solution ratio and duration), sample characteristics (*e.g.*, chemical composition and particle size), and the methods used for rate determination, etc. (Bray et al., 2015; Gudbrandsson et al., 2014; Heřmanská et al., 2022). Generally, the dissolution rates of K-feldspar and muscovite are slightly lower than those of plagioclase and biotite, respectively (Fig. 8). These trends are consistent with the inferred weathering resistance of these minerals based on natural observations (Huang et al., 2021a, b; Li and Zhou, 2020). The results show that the dissolution rates of bastnaesite are not so remarkably fast as previously speculated based on field investigation but are comparable to those of plagioclase, K-feldspars, biotite, and muscovite (Fig. 8). According to previous field studies, small amounts of clay minerals are present in the lower semi-weathered zone (Huang et al., 2021b; Li and Zhou, 2020). Therefore, we infer that during the early stage of weathering, it is highly likely that REE liberated from bastnaesite could be preserved by clay minerals formed through the decomposition of these aluminosilicates, especially plagioclase with relatively higher dissolution rates (Fig. 8). However, given the complexity of natural processes, a comprehensive evaluation of the contribution of bastnaesite to clay-adsorbed REE requires additional data, including the kinetics of clay mineral formation, the migration rates of REE, and other relevant factors for an integrated analysis. In natural settings, the preferential disappearance of bastnaesite relative to feldspars and micas in the lower part of weathering profiles might be determined by several

529 factors. Firstly, the weathering susceptibility of minerals is the dominant factor. For
530 example, K-feldspar and muscovite have relatively stronger weathering resistance and thus
531 they can even be preserved in the completely-weathered zone (Yusoff et al., 2013; Li and
532 Zhou, 2020). Additionally, the visibility of minerals across different weathering horizons
533 is also associated with their abundance in the parent rocks, with lithogenic aluminosilicates
534 generally presenting in much higher quantities than accessory phases. This may clarify why
535 plagioclase, although having a dissolution rate similar to or slightly higher than that of
536 bastnaesite (Fig. 8A), remains visible in the upper semi-weathered zones where bastnaesite
537 has almost disappeared (Huang et al., 2021a, b). Furthermore, bastnaesite and other REE
538 fluorcarbonate minerals, are typically in smaller particle sizes (commonly less than 100
539 μm) and are often distributed in cavities, cracks, or along the boundaries of the lithogenic
540 major minerals (Li et al., 2024; Sanematsu et al., 2013), enhancing their accessibility to
541 microbes and fluids, thereby promoting their dissolution (Xia et al. 2020). Our results can
542 provide some insights into the weathering of both primary and secondary REE
543 fluorcarbonate group end-members with similar chemical and crystallographic
544 characteristics to bastnaesite. As the natural REE fluorcarbonate minerals with variable
545 crystallography or chemistry, their thermodynamical stability is likely to show some
546 differences (Gysi and Williams-Jones, 2015). For instance, LREE fluorcarbonates, notably
547 bastnaesite-Ce, parisite-Ce, synchysite-Ce, are predicted to be more stable than synchysite-
548 Y in acidic environments (Li et al., 2022). Therefore, it is necessary to determine the
549 weatherability of different REE fluorcarbonates in future studies, to permit reliable
550 assessment of their potential as effective sources for the enrichment of clay-adsorbed REE
551 in the regolith-hosted REE deposits.
552

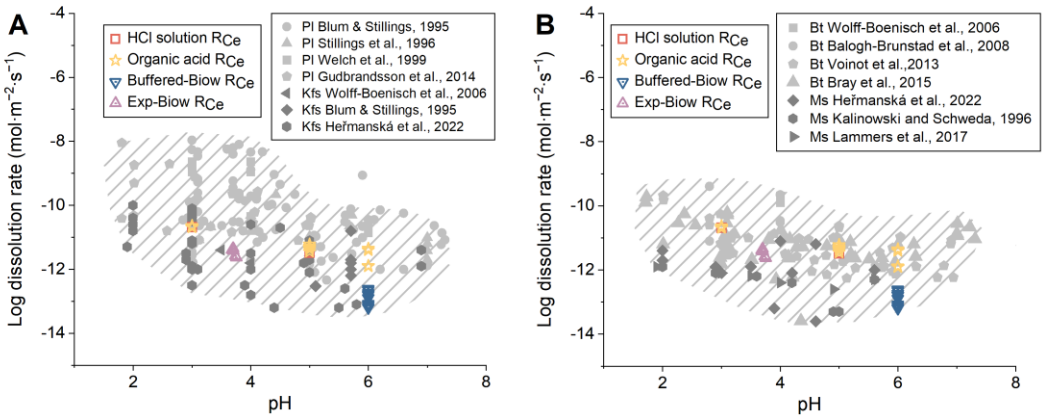

Fig. 8. Comparisons of the dissolution rates of bastnaesite (represented by R_{Ce}) in this study to those (represented by R_{Si}) of (A) plagioclase (Pl) and K-feldspars (Kfs), and (B) biotite (Bt) and muscovite (Ms) measured under similar physicochemical conditions in previous laboratory studies. The shaded area guides the eye to show the spread of literature data. Buffered-Biow R_{Ce} refers to the Ce release rates measured in the bio-weathering experiment buffered at pH = 6. The release rates of Ce from days 8 to 30 under stable acidic conditions (pH ~3.7) in the unbuffered bio-weathering experiment (Exp-Biow), as well as those measured in the abiotic chemical dissolution experiments in this study are also shown for comparison.

5. Conclusion

In this study, a wild *Bacillus* bacterium was used in bio-weathering experiments to investigate the microbial effects on the weathering of bastnaesite. The results indicate that the microbes significantly enhance bastnaesite dissolution and REE mobilization through a synergy of acidolysis and ligand complexation mechanisms under pH conditions similar to that in the regolith-hosted REE deposits. Direct microbial colonization on mineral surfaces promotes the bio-weathering performance. To the best of our knowledge, the present study is the first to report the REE release rates from natural bastnaesite. Comparisons of the dissolution rates between bastnaesite and feldspar or mica group minerals support the positive contribution of bastnaesite to the clay-adsorbed REE resource.

However, the contribution of bacterial activities to the overall weathering budgets of bastnaesite in natural soil profiles has not been quantified. Further well-designed experimental and field studies that consider diverse microbial communities, reactions at microbe-mineral interfaces, and large space and time scales in natural settings are needed to address this gap.

CRediT authorship contribution statement

Yilin He: Conceptualization, Methodology, Investigation, Writing - Original Draft, Writing - Review & Editing. **Lingya Ma:** Conceptualization, Methodology, Writing - Review & Editing, Funding acquisition. **Xurui Li:** Writing - Review & Editing. **Xun Liu:** Writing - Review & Editing, Investigation. **Xiaoliang Liang:** Funding acquisition, Resources. **Jianxi Zhu:** Funding acquisition, Resources. **Hongping He:** Supervision, Funding acquisition, Resources.

Acknowledgment

This research was financially supported by the National Natural Science Foundation of China (Grant No. 42172049); National Key R&D Program of China (Grant No. 2021YFC2901701); Science and Technology Planning Project of Guangdong Province, China (Grant No. 2023B1212060048); Science and Technology Projects in Guangzhou (Grant No. 2024A04J4827). Yilin He acknowledges the Chinese Scholarship Council (CSC) for her research scholarship (Award No. 202304910480). The authors thank Prof. Hecai Niu for his friendly donation of the bastnaesite samples.

Data availability

Data are available through Mendeley Data at https://data.mendeley.com/datasets/6n6d3fkkpc/1.

Appendix A. Supplementary data

Supplementary materials supporting this article are available online. These materials include descriptions of the methods for organic acids identification (Text S1) and mineral compositions calculation (Text S2); a summary of identified organic acids with potential bio-weathering importance (Table S1); LREE/REE ratios of dissolved REE in the experimental solutions (Figure S1); and XRD patterns of the mineral samples before and after bio-dissolution (Figure S2).

References

Adeleke, R., Nwangburuka, C., Oboirien, B., 2017. Origins, roles and fate of organic acids in soils: A review. S. Afr. J. Bot. 108, 393-406.

Ahmed, E., Holmström, S.J.M., 2015. Microbe–mineral interactions: The impact of surface attachment on mineral weathering and element selectivity by microorganisms. Chem. Geol. 403, 13-23.

Balogh-Brunstad, Z., Kent Keller, C., Thomas Dickinson, J., Stevens, F., Li, C.Y., Bormann, B.T., 2008. Biotite weathering and nutrient uptake by ectomycorrhizal fungus, Suillus tomentosus, in liquid-culture experiments. Geochim. Cosmochim. Acta 72, 2601-2618.

Bennett, P.C., Hiebert, F.K., Choi, W.J., 1996. Microbial colonization and weathering of silicates in a petroleum-contaminated groundwater. Chem. Geol. 132, 45-53.

Benzerara, K., Yoon, T.H., Menguy, N., Tyliszczak, T., Brown G.E. Jr., 2005. Nanoscale environments associated with bioweathering of a Mg-Fe-pyroxene. Proc. Natl. Acad. Sci. USA. 102, 979-982.

Blum, A., Stillings, L. 1995. Chapter 7. Feldspar dissolution kinetics, in: Chemical Weathering Rates of Silicate Minerals. Boston: De Gruyter, Berlin, pp. 291-352. doi.org/10.1515/9781501509650-009.

Bonneville, S., Morgan, D.J., Schmalenberger, A., Bray, A., Brown, A., Banwart, S.A., Benning, L.G., 2011. Tree-mycorrhiza symbiosis accelerate mineral weathering: Evidences from nanometer-scale elemental fluxes at the hypha–mineral interface. Geochim. Cosmochim. Acta 75, 6988-7005.

Borst, A.M., Smith, M.P., Finch, A.A., Estrade, G., Villanova-de-Benavent, C., Nason, P., Marquis, E., Horsburgh, N.J., Goodenough, K.M., Xu, C., Kynický, J., Geraki, K., 2020. Adsorption of rare earth elements in regolith-hosted clay deposits. Nat Commun. 11, 4386.

Bray, A.W., Oelkers, E.H., Bonneville, S., Wolff-Boenisch, D., Potts, N.J., Fones, G., Benning, L.G., 2015. The effect of pH, grain size, and organic ligands on biotite weathering rates. Geochim. Cosmochim. Acta 164, 127-145.

Brisson, V.L., Zhuang, W.-Q., Alvarez-Cohen, L., 2020. Metabolomic analysis reveals contributions of citric and citramalic acids to rare earth bioleaching by a Paecilomyces fungus. Front. Microbiol. 10, 3008.

Chistoserdova, L., 2016. Lanthanides: New life metals? World J. Microbiol. Biotechnol. 32, 138.

Davis, K.J., Nealson, K.H., Lüttge, A., 2007. Calcite and dolomite dissolution rates in the context of microbe-mineral surface interactions. Geobiology 5, 191-205.

Dong, H., Huang, L., Zhao, L., Zeng, Q., Liu, X., Sheng, Y., Shi, L., Wu, G., Jiang, H., Li, F., Zhang, L., Guo, D., Li, G., Hou, W., Chen, H., 2022. A critical review of mineral–microbe interaction and co-evolution: mechanisms and applications. Natl. Sci. Rev. 9, nwac128.

Fathollahzadeh, H., Becker, T., Eksteen, J.J., Kaksonen, A.H., Watkin, E.L.J., 2018. Microbial contact enhances bioleaching of rare earth elements. Bioresour. Technol. Rep. 3, 102-108.

Feng, M.-h., Ngwenya, B.T., Wang, L., Li, W., Olive, V., Ellam, R.M., 2011. Bacterial dissolution of fluorapatite as a possible source of elevated dissolved phosphate in the environment. Geochim. Cosmochim. Acta 75, 5785-5796.

Flemming, H.C., Wuertz, S., 2019. Bacteria and archaea on Earth and their abundance in biofilms. Nat. Rev. Microbiol. 17, 247-260.

Golubev, S.V., Pokrovsky, O.S., 2006. Experimental study of the effect of organic ligands on diopside dissolution kinetics. Chem. Geol. 235, 377-389.

Goyne, K.W., Brantley, S.L., Chorover, J., 2010. Rare earth element release from phosphate minerals in the presence of organic acids. Chem. Geol. 278, 1-14.

Gudbrandsson, S., Wolff-Boenisch, D., Gislason, S.R., Oelkers, E.H., 2014. Experimental determination of plagioclase dissolution rates as a function of its composition and pH at 22°C. Geochim. Cosmochim. Acta 139, 154-172.

Guo, D., Liu, Y., 2019. Occurrence and geochemistry of bastnäsite in carbonatite-related REE deposits, Mianning–Dechang REE belt, Sichuan Province, SW China. Ore Geol. Rev. 107, 266-282.

He, Y., Ma, L., Li, X., Wang, H., Liang, X., Zhu, J., He, H., 2023. Mobilization and fractionation of rare earth elements during experimental bio-weathering of granites. Geochim. Cosmochim. Acta 343, 384-395.

He, Y., Ma, L., Liang, X., Li, X., Zhu, J., He, H., 2024. Resistant rare earth phosphates as possible sources of environmental dissolved rare earth elements: Insights from experimental bio-weathering of xenotime and monazite. Chem. Geol. 661, 122186.

Heřmanská, M., Voigt, M., Marieni, C., Declercq, J., Oelkers, E.H., 2022. A comprehensive and internally consistent mineral dissolution rate database: Part I: Primary silicate minerals and glasses. Chem. Geol. 597, 120807.

Huang, J., He, H., Tan, W., Liang, X., Ma, L., Wang, Y., Qin, X., Zhu, J., 2021a. Groundwater controls REE mineralisation in the regolith of South China. Chem. Geol. 577, 120295.

Huang, J., Tan, W., Liang, X., He, H., Ma, L., Bao, Z., Zhu, J., 2021b. REE fractionation controlled by REE speciation during formation of the Renju regolith-hosted REE deposits in Guangdong Province, South China. Ore Geol. Rev. 134, 104172.

Kalinowski, B.E., Liermann, L.J., Brantley, S.L., Barnes, A., Pantano, C.G., 2000. X-ray photoelectron evidence for bacteria-enhanced dissolution of hornblende. Geochim. Cosmochim. Acta 64, 1331-1343.

Kalinowski, B.E., Schweda, P., 1996. Kinetics of muscovite, phlogopite, and biotite dissolution and alteration at pH 1-4, room temperature. Geochim. Cosmochim. Acta 60, 367-385.

Kelly, L., Colin, Y., Turpault, M.-P., Uroz, S., 2016. Mineral Type and Solution Chemistry Affect the Structure and Composition of Actively Growing Bacterial Communities as Revealed by Bromodeoxyuridine Immunocapture and 16S rRNA Pyrosequencing. Microb. Ecol. 72, 428-442.

Konhauser, K., 2007. Microbial weathering, in: Introduction to geomicrobiology. Blackwell Publishing, Oxford, pp. 192-234. doi.org/10.1093/acprof:oso/9780199586936.003.0013.

Lamérand, C., Shirokova, L.S., Bénézeth, P., Rols, J.-L., Pokrovsky, O.S., 2020. Olivine dissolution and hydrous Mg carbonate and silicate precipitation in the presence of microbial consortium of photo-autotrophic and heterotrophic bacteria. Geochim. Cosmochim. Acta 268, 123-141.

Lammers, K., Smith, M.K., Carroll, S.A., 2017. Muscovite dissolution kinetics as a function of pH at elevated temperature. Chem. Geol. 466, 149-158.

Li, M.Y.H., Kwong, H.T., Williams-Jones, A.E., Zhou, M.-F., 2022a. The thermodynamics of rare earth element liberation, mobilization and supergene enrichment during groundwater-regolith interaction. Geochim. Cosmochim. Acta 330, 258-277.

Li, M.Y.H., Zhou, M.-F., 2020. The role of clay minerals in forming the regolith hosted heavy rare earth

element deposits. Am. Mineral. 105, 92-108.

Li, M.Y.H., Zhou, M.-F., 2024. Hyper-enrichment of heavy rare earth elements in highly evolved granites through multiple hydrothermal mobilizations. Am. Mineral. 109, 1945-1959.

Li, M.Y.H., Zhou, M.-F., Williams-Jones, A., 2020. Controls on the Dynamics of Rare Earth Elements During Subtropical Hillslope Processes and Formation of Regolith-Hosted Deposits. Econ. Geol., 115, 1097-1118.

Li, M.Y.H., Zhou, M.-F., Williams-Jones, A.E., 2019a. The Genesis of Regolith-Hosted Heavy Rare Earth Element Deposits: Insights from the World-Class Zudong Deposit in Jiangxi Province, South China. Econ. Geol. 114, 541-568.

Li, X., Liang, X., He, H., Li, J., Ma, L., Tan, W., Zhong, Y., Zhu, J., Zhou, M., Dong, H., 2022b. Microorganisms accelerate REE mineralization in supergene environments. Appl. Environ. Microbiol. 88, e0063222.

Li, Z.-b., Liu, L., Lu, X., Ji, J., Chen, J., 2021. Analysis of the Talaromyces flavus exometabolome reveals the complex responses of the fungus to minerals. Geochim. Cosmochim. Acta 298, 70-86.

Li, Z.-b., Lu, X., Teng, H.H., Chen, Y., Zhao, L., Ji, J., Chen, J., Liu, L., 2019b. Specificity of low molecular weight organic acids on the release of elements from lizardite during fungal weathering. Geochim. Cosmochim. Acta 256, 20-34.

Li, Z., Liu, L., Chen, J., Teng, H.H., 2016. Cellular dissolution at hypha- and spore-mineral interfaces revealing unrecognized mechanisms and scales of fungal weathering. Geology 44, 319-322.

Liermann, L.J., Kalinowski, B.E., Brantley, S.L., Ferry, J.G., 2000. Role of bacterial siderophores in dissolution of hornblende. Geochim. Cosmochim. Acta 64, 587-602.

Migdisov, A., Williams-Jones, A.E., Brugger, J., Caporuscio, F.A., 2016. Hydrothermal transport, deposition, and fractionation of the REE: Experimental data and thermodynamic calculations. Chem. Geol. 439, 13-42.

Minyard, M.L., Bruns, M.A., Liermann, L.J., Buss, H.L., Brantley, S.L., 2012. Bacterial Associations with Weathering Minerals at the Regolith-Bedrock Interface, Luquillo Experimental Forest, Puerto Rico. Geomicrobiol. J. 29, 792-803.

Morse, J.W., Arvidson, R.S., 2002. The dissolution kinetics of major sedimentary carbonate minerals. Earth-Sci. Rev. 58, 51-84.

Napieralski, S.A., Buss, H.L., Brantley, S.L., Lee, S., Xu, H. and Roden, E.E., 2019. Microbial chemolithotrophy mediates oxidative weathering of granitic bedrock. Proc. Natl. Acad. Sci. USA 116, 26394-26401.

Pan, Y., Fleet, M.E., 2002. Compositions of the Apatite-Group Minerals: Substitution Mechanisms and Controlling Factors. Rev. Mineral. Geochem. 48, 13-49.

Purkamo, L., Bomberg, M., Kietäväinen, R., Salavirta, H., Nyyssönen, M., Nuppunen-Puputti, M., Ahonen, L., Kukkonen, I. and Itävaara, M., 2016. Microbial co-occurrence patterns in deep Precambrian bedrock fracture fluids. Biogeosciences 13, 3091-3108.

Rather, M.A., Gupta, K., Mandal, M., 2021. Microbial biofilm: formation, architecture, antibiotic resistance, and control strategies. Braz. J. Microbiol. 52, 1701-1718.

Samuels, T., Bryce, C., Landenmark, H., McLean, C., Nicholson, N., Stevens, A., Cockell, C., 2020. Microbial Weathering of Minerals and Rocks in Natural Environments, In: Biogeochemical Cycles: Ecological drivers and environmental impact. Wiley & Sons, Inc., Hoboken, pp:59-79. doi.org/10.1093/acprof:oso/9780199586936.003.0013.

Sanematsu, K., Kon, Y., Imai, A., Watanabe, K., Watanabe, Y., 2013. Geochemical and mineralogical characteristics of ion-adsorption type REE mineralization in Phuket, Thailand. Miner. Deposita 48, 437-451.

Sanematsu, K., Watanabe, Y., 2016. Characteristics and genesis of ion adsorption-type rare earth element deposits. Rev. Econ. Geol. 18, 55-79.

Sarrah, M.D.-C., You, Y., 2019. Standard techniques in geomicrobiology. In: Kenney, J.P. L., Veeramani, H., Alessi, D.S. (Eds.), Analytical Geomicrobiology a Handbook of Instrumental Techniques. Cambridge University Press, Cambridge, pp. 1-60.

Schmalenberger, A., Duran, A., Bray, A., Bridge, J., Bonneville, S., Benning, L.G., Romero-Gonzalez, M.E., Leake, J.R., Banwart, S.A., 2015. Oxalate secretion by ectomycorrhizal Paxillus involutus is mineral-speciffc and controls calcium weathering from minerals. Sci. Rep. 5.

Sheng, Y., Baars, O., Guo, D., Whitham, J., Srivastava, S., Dong, H., 2023. Mineral-Bound Trace Metals as Cofactors for Anaerobic Biological Nitrogen Fixation. Environ. Sci. Technol. 57, 7206-7216.

Shi, A., Xu, C., Fan, C., Chakhmouradian, A.R., Brenna, M., Wei, C., 2024. Structural Defects of Heavy Rare Earth Element Minerals in Granite Accelerate Their Decomposition and Facilitate Mineralization During Weathering. Econ. Geol. 119, 871-883.

Shibata, S.-N., Tanaka, T., Yamamoto, K., 2006. Crystal structure control of the dissolution of rare earth elements in water-mineral interactions. Geochem. J. 40, 437-446.

Shirokova, L.S., Bénézeth, P., Pokrovsky, O.S., Gerard, E., Ménez, B., Alfredsson, H., 2012. Effect of the heterotrophic bacterium *Pseudomonas reactans* on olivine dissolution kinetics and implications for CO_2 storage in basalts. Geochim. Cosmochim. Acta 80, 30-50.

Shivaramaiah, R., Anderko, A., Riman, R.E., Navrotsky, A., 2016. Thermodynamics of bastnaesite: A major rare earth ore mineral. Am. Mineral. 101, 1129-1134.

Stillings, L.L., Drever, J.I., Brantley, S.L., Sun, Y., Oxburgh, R., 1996. Rates of feldspar dissolution at pH 3–7 with 0–8 mM oxalic acid. Chem. Geol. 132, 79-89.

Strobel, B.W., 2001. Influence of vegetation on low-molecular-weight carboxylic acids in soil solution—a review. Geoderma 99, 169-198.

Uroz, S., Oger, P., Lepleux, C., Collignon, C., Frey-Klett, P., Turpault, M.-P., 2011. Bacterial weathering and its contribution to nutrient cycling in temperate forest ecosystems. Res. Microbiol. 162, 820-831.

Voinot, A., Lemarchand, D., Collignon, C., Granet, M., Chabaux, F., Turpault, M.P., 2013. Experimental dissolution vs. transformation of micas under acidic soil conditions: Clues from boron isotopes. Geochim. Cosmochim. Acta 117, 144-160.

Welch, S.A., Barker, W.W., Banfield, J.F., 1999. Microbial extracellular polysaccharides and plagioclase dissolution. Geochim. Cosmochim. Acta 63, 1405-1419.

Weng Q., Yang W., Niu H., Li N., Mitchell R.H., Zurevinski S., Wu D., 2022. Formation of the Maoniuping giant REE deposit: Constraints from mineralogy and in situ bastnäsite U-Pb geochronology. Am. Mineral. 107, 282-293.

Wild, B., Gerrits, R., Bonneville, S.C., 2022. The contribution of living organisms to rock weathering in the critical zone. npj Mater. Degrad. 6, 98.

Williams-Jones, A.E., Samson, I.M., Olivo, G.R., 2000. The Genesis of Hydrothermal Fluorite-REE Deposits in the Gallinas Mountains, New Mexico. Econ. Geol. 95, 327-341.

Williams-Jones, A.E., Wood, S.A., 1992. A preliminary petrogenetic grid for REE fluorocarbonates and associated minerals. Geochim. Cosmochim. Acta 56, 725-738.

Wolff-Boenisch, D., Gislason, S.R., Oelkers, E.H., 2006. The effect of crystallinity on dissolution rates and CO_2 consumption capacity of silicates. Geochim. Cosmochim. Acta 70, 858-870.

Wu, L., Jacobson, A.D., Hausner, M., 2008. Characterization of elemental release during microbe–granite interactions at T=28°C. Geochim. Cosmochim. Acta 72, 1076-1095.

Yang, Y., Li, G., Huang, C., Liu, X., Wang, X., Li, C., Wu, B., Luo, W., 2023. Discovery of supergene REE-fluorocarbonate minerals in weathered spheres of Xiajialing regolith-hosted rare earth element deposit in Xiangshan, Jiangxi Province, South China. Ore Geol. Rev. 162, 105712.

Yusoff, Z.M., Ngwenya, B.T., Parsons, I., 2013. Mobility and fractionation of REEs during deep weathering of geochemically contrasting granites in a tropical setting, Malaysia. Chem. Geol. 349-350, 71-86.

Zhang, L., Dong, H., Liu, Y., Bian, L., Wang, X., Zhou, Z., Huang, Y., 2018. Bioleaching of rare earth elements from bastnaesite-bearing rock by actinobacteria. Chem. Geol. 483, 544-557.483: 544-557.

Table 1 Chemical compositions of the bastnaesite sample.

Oxides	%	Elements	$mg \cdot kg^{-1}$
CeO_2	36.1	Eu	463
La_2O_3	30.1	Gd	806
Nd_2O_3	7.40	Tb	84.4
Pr_6O_{11}	2.57	Dy	121
SiO_2	0.635	Ho	11.9
Na_2O	0.450	Y	252
MgO	0.335	Er	21.0
Sm_2O_3	0.275	Tm	1.24
ThO_2	0.246	Yb	10.1
LOI	20.5	Lu	0.545

Table 2 Log apparent release rates ($mol \cdot m^{-2} \cdot s^{-1}$) of La, Ce, Pr, Nd, and total REE in the bio-weathering experiment buffered at pH = 6. The standard deviation was calculated from triplicate samples.

Time (day)	La	Ce	Pr	Nd	Total REE
1	−12.74 ± 0.08	−12.41 ± 0.07	−13.45 ± 0.04	−12.89 ± 0.05	−12.08 ± 0.06
2	−12.80 ± 0.01	−12.52 ± 0.01	−13.52 ± 0.04	−12.96 ± 0.03	−12.17 ± 0.02
4	−12.61 ± 0.04	−12.37 ± 0.05	−13.41 ± 0.04	−12.90 ± 0.03	−12.04 ± 0.04
6	−12.66 ± 0.07	−12.44 ± 0.05	−13.48 ± 0.04	−12.96 ± 0.03	−12.11 ± 0.05
8	−12.79 ± 0.08	−12.54 ± 0.06	−13.56 ± 0.05	−13.05 ± 0.04	−12.21 ± 0.06
10	−12.90 ± 0.03	−12.63 ± 0.02	−13.64 ± 0.02	−13.12 ± 0.03	−12.31 ± 0.02
15	−13.07 ± 0.01	−12.76 ± 0.01	−13.77 ± 0.00	−13.23 ± 0.01	−12.44 ± 0.01
20	−13.13 ± 0.07	−12.83 ± 0.05	−13.84 ± 0.03	−13.32 ± 0.02	−12.52 ± 0.04
25	−13.19 ± 0.04	−12.90 ± 0.02	−13.91 ± 0.03	−13.38 ± 0.04	−12.59 ± 0.01
30	−13.20 ± 0.03	−12.89 ± 0.03	−13.90 ± 0.02	−13.39 ± 0.02	−12.59 ± 0.03